The influence of thermo-mechanics in the catastrophic collapse of planar landslides

Francesco Cecinato[1] and Antonis Zervos

Faculty of Engineering and the Environment, University of Southampton

Highfield, SO17 1BJ Southampton, UK

francesco.cecinato@gmail.com

az@soton.ac.uk

[1] Currently at ENI, E&P Division, Geomechanics Laboratory (LAIP). Via Maritano 26, 20097 S. Donato Milanese (Milan), Italy. Email: francesco.cecinato@eni.com

ABSTRACT

Frictional heating has long been considered a mechanism responsible for the high velocities and long run-out of some large-scale landslides. In this work a landslide model is presented, applicable to planar large-scale landslides occurring in a coherent fashion. The model accounts for temperature rise in the slip zone due to the heat produced by friction, leading to water expansion, thermoplastic collapse of the soil skeleton and subsequently to an increase of pore water pressure. The landslide model, comprising equations that describe heat and pore pressure diffusion and the dynamics of the moving mass, is used to analyse the evolution of the Jiufengershan planar landslide as an example. Further, its parameter space is systematically but efficiently explored using a Taguchi parametric analysis in an attempt to quantify dominant parameters. It is shown that the process of sliding is dominated by the softening properties of the material, as expected, but also by the permeability of the slip zone and the thickness of the sliding mass. It is worth noting that the latter two parameters do not enter traditional stability analyses of uniform slopes.

Key words: thermal pressurization, landslide dynamics, numerical analysis, thermo-mechanics, Taguchi methods, parametric study

1. INTRODUCTION

Frictional heating has long been considered one of the possible key phenomena behind the rapid, substantial loss of shear strength occurring in the slip zone of some large scale landslides, leading to unconstrained acceleration (Habib 1975, Voight and Faust 1982). Pore pressure in soils increases with temperature due to thermal expansion and the eventual thermal collapse of the skeleton (Hueckel and Pellegrini 1991, Modaressi and Laloui 1997, Hueckel and Baldi 1990), especially under conditions of slow or no drainage, like the ones occurring in the rapidly deforming slip zone of a landslide. Moreover, heating reduces the soil's apparent overconsolidation ratio, shrinks its elastic domain and lowers its peak stress ratio (Hueckel and Baldi 1990, Laloui and Cekerevac 2003). These processes lead to declining shear resistance at the slip zone, causing the sliding mass to accelerate and potentially making the difference between a relatively low-impact event and a catastrophic one.

The first comprehensive landslide model accounting for frictional heating and thermal pressurization in the slip plane of a uniform slope was presented by Vardoulakis (2000, 2002). However the specialized constitutive law it used for the soil cannot capture the full range of temperature-dependent soil behaviour observed experimentally, and it cannot be easily generalized to include the behaviour of the soil prior to failure, or to model two- or three-dimensional problems.

Cecinato et al. (2008, 2011) further developed Vardoulakis' (2002) model by adopting a more general constitutive assumption for the soil, applicable to a wider range of soils. This was done by adopting a thermo-plastic Modified Cam Clay constitutive framework, in which strain-, strain rate- and thermal softening could be accommodated. It was shown that contrary to what may have been expected, the introduction of thermal softening did not

lead to ill-posedness of the governing equations. It was also possible to determine the pressurisation coefficient in terms of other, better established material parameters and state variables, rather than consider it an independent parameter.

In this work, the model equations of Cecinato et al. (2011) describing heat generation and diffusion, pore pressure generation and dissipation, and the thermo-mechanical behaviour of soil are outlined, in the framework of an infinite slope geometry. The model is then employed to simulate as an example the collapse of the large-scale planar landslide of Jiufengershan (e.g., Chang et al. 2005), showing that realistic sliding velocity estimates can be obtained. A parametric analysis is subsequently carried out, to identify the dominant parameters (among different geometrical characteristics and soil properties) that make an infinite slope prone to catastrophic collapse. To improve the efficiency of the parametric study and explore significant parameter combinations only, the statistical-based Taguchi experimental design method (e.g. Taguchi et al., 1989, Peace, 1993) is adopted. Through this procedure the main factors which maximise the predicted slide velocity, i.e. those exacerbating the catastrophic character of the slide, are identified and ranked.

In the following, we present in Section 2 the soil constitutive model and in Section 3 the formulation of the landslide model. In Section 4 the analysis of the Jiufengershan landslide is discussed and in Section 5 we describe a general parametric study involving 13 parameters. In Section 6 the significance of thermo-mechanical properties in particular is explored; and conclusions are summarized in Section 7.

2. CONSTITUTIVE MODEL

2.1 Thermo-plastic behaviour of soil

Temperature influences the behavior of clays by causing volume variations of the free water and by changing the adsorption forces in the structural water (Sulem et al. 2007).

Such effects are reflected in volumetric strains caused by heating, which are mainly reversible and dilative if the soil is over-consolidated, and irreversible and contractive if the soil is normally-consolidated (Hueckel and Baldi 1990, Laloui et al. 2005). Another typical feature of clays is thermal softening, i.e. a reduction of the size of the elasticity domain of the soil as temperature increases (Laloui and Cekerevac 2003).

The first model on the thermal response of soils was proposed by Campanella and Mitchell (1968) and formed the basis for several subsequent constitutive studies; notably Hueckel and Borsetto (1990) described the thermo-plasticity of saturated soils and shales, and more recently Laloui and Cekerevac (2003) proposed a model to describe the volumetric response of clay to heating, which was then extended to a multi-mechanism framework (Laloui et al. 2005, Laloui and Francois 2009). Based on these ideas, Cecinato et al. (2011) described the development of a constitutive model of the Cam Clay family able to capture the main features outlined above, in the context of a rapidly deforming clayey shearband subject to frictional heating. The core aspects of this model are summarized here for completeness.

The Modified Cam Clay model (Roscoe and Burland 1968) was adopted as it is a widely used model with clear advantages when it comes to numerical implementation. The yield surface is expressed in terms of the mean effective stress p' and the deviatoric stress q:

[1] $$f = q^2 - M^2 p'\left(\sigma_c' - p'\right)$$

where M the critical state parameter and associated plastic flow is assumed.

The thermal softening/hardening response of the volumetric behaviour of soil is described by the hardening rule proposed by Laloui and Cekerevac (2003) where the apparent preconsolidation stress σ_c', corresponding to the intersection of the yield surface with the mean effective stress axis, is a function of temperature:

[2] $$\sigma'_c = \sigma'_{c0} \exp(\tilde{\beta}\varepsilon_v^p)\left[1 - \gamma \log\left(\theta/\theta_{ref}\right)\right]$$

In the above, σ'_{c0} is the isothermal value of the preconsolidation stress, $\tilde{\beta}$ the plastic compressibility, ε_v^p the accumulated volumetric plastic strain, γ a material parameter representing the rate of softening and θ and θ_{ref} the current and reference values of temperature respectively.

Another feature that has been observed in some clays is thermal-friction softening, i.e. the dependence on temperature of the friction angle at critical state ϕ'_{cs}. However there is no clear consensus in the literature, as both the existence of this effect and its nature appear to be material-dependent (Marques et al. 2004, Laloui et al. 2005, Sulem et al. 2007). To allow for the possibility of thermal-friction softening, which may be a mechanism contributing to the destabilization of a sliding mass, the linear law proposed by Laloui et al. (2005) is adopted:

[3] $$M = M_{ref} - \tilde{g}\left(\theta - \theta_{ref}\right)$$

where M_{ref} is the value of critical state parameter at the reference temperature θ_{ref}, and $\tilde{g}$ represents the rate of thermal friction softening.

2.2. Thermal pressurization mechanism

Thermal pressurization due to frictional heating has been studied in a number of different contexts (Sibson 1973, Lachenbruch 1980, Vardoulakis 2000, 2002, Wibberley and Shimamoto 2005, Rice 2006, Sulem et al. 2007), while experimental evidence for both rocks and soils is also available (Campanella and Mitchell 1968, Baldi et al. 1988, Sultan 1997, Sultan et al. 2002, Ghabezloo and Sulem 2008). The key parameter governing

thermal pressurization is the pressurization coefficient λ_m, defined as the pore pressure increase due to a unit temperature increase in undrained conditions. Its value depends on the material, the temperature and the stress level. Different average values for λ_m have been proposed for clay, ranging between 0.01 MPa/°C and 0.1 MPa/°C. As shown in Cecinato et al (2011), within the framework of the constitutive model presented above a gradual collapse of the soil skeleton is predicted and it is possible to determine the pressurization coefficient λ_m as a function of the temperature, the void ratio and the soil constants:

[4] $$\lambda_m(\theta) = -\frac{1}{c}\frac{\lambda-\kappa}{\lambda}\left\{\frac{\gamma\ \kappa}{(1+\mathrm{e})\theta\left[1-\gamma\log\left(\theta/\theta_{ref}\right)\right]}-2\beta_s\right\}$$

where λ and κ are the (dimensionless) slope of the normal-compression line and the unloading-reloading line of the soil respectively, *e* is the void ratio and c is the oedometric compressibility, which can be determined in terms of other material parameters (Cecinato et al. 2011). The pressurization coefficient λ_m must be positive to be physically meaningful.

3. THE LANDSLIDE MODEL

The geometry of a considered landslide is divided into two regions: the shear-band, which is a thin zone where all deformation is localized and which is embedded in a thicker soil layer, and the overburden, which moves as a rigid block (Figure 1). The thickness of the shearband is assumed constant and may be empirically related to the mean grain size of the geomaterial (Vardoulakis 2002).

The considered analysis starts at incipient failure, thus we assume that the soil within

the shearband has already reached critical state. Furthermore, plane strain conditions are assumed along the *y* axis. The *x* axis points in the direction of movement and the *z* axis is taken perpendicular to it. A linear profile of velocity within the shearband is assumed (Vardoulakis 2001), while the bulk of the slide moves as a rigid body with a speed $v_d(t)$. Velocity and acceleration along the z axis are considered negligible. The small, compared to the slide dimensions, thickness of the band allows for all variations in the direction of sliding to be neglected, so that temperature and pore pressure changes occur along the *z*-direction only.

3.1 Heat equation

This is derived from energy balance, and describes the evolution of temperature θ within the shearband (Cecinato et al. 2008, 2011) :

[5] $$\frac{\partial \theta}{\partial t} = D_i \frac{\partial^2 \theta}{\partial z^2} + F_i \frac{v_d(t)}{d}$$

where $v_d(t)$ is the velocity at the upper boundary of the shearband, also corresponding to the sliding velocity of the rigid block. The coefficients $D_i(\theta, u, \gamma, \dot{\gamma})$ and $F_i(\theta, u, \gamma, \dot{\gamma})$ depend on pore pressure *u*, temperature θ and on the shear strain γ and strain rate $\dot{\gamma}$ (Cecinato et al. 2011). Both thermal-friction softening and displacement- and velocity-friction softening of the soil in the shearband are taken into account (see Appendix).

Equation [5] is a diffusion-generation equation for the temperature where the diffusivity coefficient D_i varies non-linearly with temperature and pore pressure. Extensive numerical experimentation showed D_i to vary very little and to be positive for a wide range of values of the parameters involved (Cecinato et al. 2008, Cecinato 2009, 2011), therefore the problem remains well-posed from the mathematical point of view.

3.2 Pore pressure equation

The pore pressure equation is derived from mass balance considerations and Darcy's law, and describes the time evolution of excess pore pressures within the shearband and the surrounding soil due to thermal pressurization and flow:

[6] $$\frac{\partial u}{\partial t} = \bar{c}_v \frac{\partial^2 u}{\partial z^2} + \lambda_m \frac{\partial \theta}{\partial t}$$

In the above $\bar{c}_v$ is the average consolidation coefficient:

[7] $$\bar{c}_v = \frac{k_w}{g \rho_w c}$$

where *c* is the soil compressibility, *g* the acceleration of gravity, ρ_w the pore-fluid density and k_w is Darcy's permeability coefficient.

3.3 Dynamic equation of the sliding mass

To complete the description of the phenomena, an equation for the dynamics of the sliding mass is needed. Here attention is given to planar sliding, appropriate for translational landslides in which the rupture surface can be assumed, with reasonable approximation, parallel to the surface of the slope. The case of rotational sliding, which is an appropriate assumption for deep-seated slides where the slip surface can be approximated as circular, is treated elsewhere (Cecinato et al., 2011)

Within the framework of an infinite slope geometry, shown in Figure 1, the slope is assumed uniform and of unlimited extent. The slip plane is parallel to the surface of the slope at depth *H*. A unit length of slope is considered and, for a given geometry, gravity and seepage forces determine the safety factor in static analyses, or the acceleration in

post-failure, dynamic analyses. Dynamic equilibrium of the unit length block of Figure 1 leads to the dynamical equation:

[8] $$\frac{dv_d}{dt} = g\left[\sin\beta - \frac{\tau_{zx}(t)}{\gamma_s H}\right]$$

In the above, v_d is the velocity of the block, g the acceleration of gravity, β the slope angle, γ_s the unit weight of the soil and $\tau_{zx}(t)$ the shear stress in the shearband. The latter, together with the block velocity, provides the coupling between the shearband constitutive model and the dynamical equation, and it can be expressed according to a conventional Mohr-Coulomb frictional law as:

[9] $$\tau_{zx}(t) = \sigma'_n(t)\cdot\tan\left(\varphi'_{cs}\right)$$

where $\varphi'_{cs}(t) = \varphi'_{cs}(\gamma,\dot{\gamma},\theta)$ is the (potentially softening with strain, strain rate and temperature) friction angle and $\sigma'_n(t) = \sigma'_{n0} - u(t)$ the current normal effective stress. The latter can be written in terms of the mean effective stress p', under the simplifying assumption that $\sigma'_{xx} = \sigma'_{yy}$ (Cecinato et al., 2011), as

[10] $$\sigma'_n = 3\left(\frac{1-\nu}{1+\nu}\right)p'$$

where p' the current mean effective stress and ν the Poisson ratio of the soil.

Equation [8] can be adopted to interpret the dynamics of the collapse of a planar landslide coupled with the shearband governing equations [5] and [6]. The coupling variables are the

slide velocity $v_d(t)$, the average pore pressure at the shearband-block interface $u_d(t)$ and the friction angle $\varphi'_{cs}(t) = \varphi'_{cs}(\gamma, \dot{\gamma}, \theta)$.

3.4 Outline of the numerical treatment

The coupled equations [5], [6] and [8] were discretized using a finite difference scheme and integrated numerically to determine the evolution of temperature, excess pore pressure and slide velocity with time. The heat and pore pressure equations were discretized using a Forward-Time Centered-Space explicit finite difference scheme. Stability was ensured by controlling the size of the time-step on the basis of a von Neumann-type stability analysis and numerical experimentation. Equation [8] was discretized with a standard fourth-order Runge-Kutta scheme using the same time-step.

The shearband is assumed to be embedded in a clay layer of the same characteristics, whose thickness is much larger than the shearband thickness *d*. Shear straining and consequent heat production occur within the shearband only. The extent of the spatial domain modelled was 10 times the thickness of the shearband and it was assumed to be uniform in hydraulic, thermal and geotechnical properties. This distance was assumed sufficiently large for the excess pore pressure there to be considered zero and for the temperature to be equal to the ambient value.

4. NUMERICAL EXAMPLE: THE JIUFENGHERSHAN LANDSLIDE

4.1. Main features of the slide

As an example, the above model is applied to the case history of the landslide of Jiufengershan (Shou and Wang, 2003, Wang et al., 2003, Chang et al., 2005). This particular landslide was chosen because a) it had, with good approximation and over a relatively long distance, a planar slip surface, b) a number of field data are available which,

although limited, are adequate for a first-approximation simulation, and c) there was direct field evidence for the development of both high temperatures and high excess pore pressures in the course of sliding.

The Jiufengershan landslide was triggered by the 1999 Chi-Chi earthquake in Taiwan. It affected weathered rock and soil materials, which quickly slid along the bedding plane, initially in a coherent manner and subsequently in a flow-like fashion (Chang et al. 2005), for a total displacement of 1 km. The slip surface developed along a pre-existing bedding fault, constituted of alternating beds of dark gray shale and muddy sandstone. Bedding-parallel clay seams of 1-6 cm in thickness were found in the slip plane throughout the slope, with clear slickensides and dip-slip striations (Wang et al. 2003). The occasional presence of pseudotachylytes (glassy material resulting from rock melting) implies a sliding velocity so high that, locally, the rock must have been heated to temperatures in excess of 1000 °C, presumably at locations of the slip plane where direct rock-to-rock contact was possible (Chang et al. 2005). We can then reasonably expect similar sliding-induced heat production to have taken place within the clay as well, although of a lower order of magnitude. Furthermore, there was field evidence of pore water pressurisation in the shear zone, as adjacent rock joints were recorded to be “filled with sheared mud” (Chang et al. 2005). This is compatible with the occurrence of pore water pressurization in the course of sliding.

Based on the above observations, Chang et al. (2005) proposed a simple block-on-slope model to simulate the landslide dynamics accounting for thermal effects. To provide a more comprehensive understanding of the thermomechanics of the landslide and of the extent to which different parameters of the problem could have affected it, the infinite slope model presented in Section 3 is employed to investigate the final collapse phase.

4.2. Choice of parameters

The available field data on the Jiufengershan slide, reported by Chang et al. (2005), Shou and Wang (2003) and Wang et al. (2003), are given in Table 1. In Table 1 parameter *d* has been assigned the value of 1 cm as a reasonable mid-range value for the thickness of the shearband, which was found to vary between extremes of 1 mm and 10 cm (Chang et al. 2005). The water table height is assigned the average value h_w=30 m after Chang et al. (2005), implying within the framework of an infinite slope geometry, that the flow lines are assumed parallel to the slope.

The reported field observations (Huang et al. 2001) suggest that the slip occurred along the bedding plane separating the Changhuken formation (shale interbedded with thin sandstone layers) and the Shihmen formation (thick sandstone). The presence of clayey layers with clear slip striations intercalated between the aforementioned rock formations (Wang et al. 2003) suggests that the slip occurred at the interface between rock and the clay seams, similarly to the Vajont case (Hendron and Patton 1985). It will be therefore assumed that deformation was localised within one of the clay layers. However, no information is available on the geotechnical properties of the clay. In this case the friction angle at critical state may be calculated through limit equilibrium conditions with the field data of Table 1, resulting to $\phi'_{cs} = 27.4°$ at incipient failure. By considering equilibrium of forces in *z* direction, the initial normal effective stress is calculated as $\sigma_n' = 0.876$ MPa. In the absence of site-specific data, the clay properties κ, λ and Γ, respectively defining the slope of the elastic recompression line, the slope of the isotropic normal compression line and the specific volume intercept of the critical state line, are assigned mid-range values from a range of known values for different clays (Schofield and Wroth, 1968, Wood et al. 1992). The thermo-mechanical properties of the soil, namely the thermo-elastic expansion coefficient β_s, the thermal diffusivity k_m and the thermal constant C_f do not vary

significantly for different types of soil (cf. Alexandre et al. 1999, Vardoulakis, 2002) and are assigned typical values (Cecinato et al. 2011). The reference temperature θ_{ref} can be set to 25°C as reported by Chang et al. (2005), reflecting the climate of Taiwan. Water compressibility is set to the average value of 4.9×10^{-4} MPa^{-1} (cf. Vardoulakis 2002).

In the absence of direct measurements the soil permeability is set to a value $k_w = 10^{-11}$ m/s, representative of clayey soils (cf. Vardoulakis 2002). The thermal softening parameter γ is assigned the lower-mid-range value $\gamma = 10^{-2}$ (Cecinato et al. 2011). Furthermore, since no information is available on the friction-softening properties of the Jiufengershan soil, the friction angle is set constant for a first-attempt simulation.

The above discussed parameters are summarised in Table 2.

4.3. Numerical results and discussion

It should be noted that the thermo-mechanical landslide model can interpret the final catastrophic acceleration phase, however it cannot be employed to simulate the 'stick-slip behaviour' which is typical of the co-seismic inertial displacements (Chang et al. 2005). Due to prolonged earthquake shaking (more than 30 seconds based on the available accelerogram records, cf. Huang et al. 2001) one may assume that the soil in the shearband reached failure in an undrained manner (Cecinato 2009, 2011) while the temperature at the base of the slide increased, due to frictional heating, from the ambient value of θ_{ref}=25°C. A value of $\theta_0 = 45\,°C$, as calculated by Chang et al. (2005) through a Newmark-type analysis (Newmark, 1965) modified to include thermo-mechanical considerations, is adopted as the shearband temperature at the onset of catastrophic collapse.

The final collapse phase of Jiufengershan is simulated by numerically integrating the landslide model of Section 3 using the above parameter values and initial conditions. The initial velocity is set to zero and sliding is numerically initiated by a minute reduction of the friction angle.

Temperature and excess pore pressure isochrones were produced for a time window of 20 seconds after initiation (Figure 2 and Figure 3). It can be seen that after 10s from initiation, at the shearband mid-plane $\theta \approx 55$°C and $u \approx 60$kPa. In both graphs, the flat profile of the isochrones within the shearband for t=20s reveals the asymptotic convergence to a steady state for heat production: temperature reaches a maximum value $\theta_{max} \approx 134$°C as the shearband soil liquefies due to full pressurisation and the shear stress tends to zero. This is best illustrated in Figure 4, where the computed excess pore pressure and shear stress at the shearband mid-plane are plotted against time: the weakening of shear resistance is closely related to the rise of excess pore pressure, and the rates of both tend to zero after t=18s.

In Figure 5 the slide velocity and displacement are plotted against time. At t=10s, a velocity of 0.9m/s is reached after 1.5m displacement. A rapid acceleration follows, such that only 10 seconds later (at t=20s) the landslide attains the catastrophic velocity of 25 m/s.

Field observations suggest that the maximum displacement of the Jiufengershan slide was 1 km (Chang et al. 2005). The maximum velocity reached by the slide was estimated by Chang et al. (2005) to be about 80 m/s, at a stage when the mass could have lost its integrity and moved in a flow-like fashion. Nevertheless, this later-stage evolution appears to be well reproduced with the above presented landslide model: by extending the simulations to a time of 40 seconds after initiation (Figure 6), a velocity of about 80 m/s is calculated after a displacement of 1000m.

4.4. Impact of friction softening and shearband thickness

The effects of possible material friction-softening and of a a thinner shearband in the Jiufengershan simulations are explored hereafter. As an example it may be assumed that the static residual friction angle for the Jiufengershan clay is around 10°, as is typical of soils with significant clay fraction (Skempton 1985). For simplicity, the friction angle is

allowed to decrease with displacement only, assuming for the rate of static friction softening, in the absence of better information, the value reported in Vardoulakis (2002).

Calculations were carried out for a total time window of 20 seconds. The resulting temperature and pore pressure isochrones are very similar to those presented in Section 4.3, but the effect of the rapid decrease of friction with displacement is evident in the variable slope of the shear stress plot (Figure 7): an initial, very steep branch due to friction softening is followed by a relatively milder one, representing the continuation of the shear resistance weakening due to pressurisation, towards the asymptotic attainment of a liquefied state after t=12s. By comparing the shear stress and excess pore pressure plots of Figure 7 to those in Figure 4 it can be seen that pressurisation now occurs sooner, due to faster frictional heating (Figure 8). In fact the velocity and acceleration are heavily affected by material softening, as the slide reaches 500m at a speed of almost 60 m/s 20 seconds after initiation (Figure 9).

The effect of the shearband thickness on the slide dynamics is investigated by choosing for d the lower-range value of 1mm (Chang et al. 2005) all other parameters being equal: more localised shearing causes heating and pressurisation to be more concentrated around the shearband mid-plane (Figure 10 and Figure 11). Also, thermal pressurisation happens faster, as in this case full pressurisation is attained after only 8s (Figure 12). The acceleration is also higher, as velocity reaches about 50 m/s at t=20s (Figure 13).

5. PARAMETERS GOVERNING CATASTROPHIC COLLAPSE

The general difficulty in finding a sufficient number of reliable geotechnical parameters from landslide case histories brings about a significant degree of uncertainty in the model predictions. To overcome this difficulty, the influence of each of the different parameters on the response of the system should be assessed, to determine their relative importance

and allow prioritization of the field and laboratory measurements that deserve most attention. To meet this purpose, in this section the landslide model is employed to carry out a general parametric study, with the aim of identifying the most important parameters that may make a slope prone to catastrophic failure. This is done through a number of simulations where each relevant geometrical and geomechanical property of the slide is independently varied within realistic ranges.

Due to the wide variety of contexts in which landslides occur, there is no unique definition of what constitutes a 'catastrophic' slide. Nevertheless, a criterion to formally distinguish between catastrophic and non-catastrophic cases could still be established, based on the velocity reached by a slide after a certain distance. For example, one could consider as catastrophic any landslide which after 10 metres of displacement, reaches a velocity of 3 m/min (i.e., 0.05 m/s) or more. The latter value constitutes the threshold velocity for 'very rapid' slides in the IUGS (1995) velocity classification; while 10 metres can arguably, although rather arbitrarily, be considered, in first approximation, a distance large enough for a slide to be noticed, but perhaps depending also on the context, small enough to avoid major damage. Alternatively, one could use as a criterion of ranking how catastrophic a landslide can be the velocity reached after 10 seconds from initiation, a small enough value to save computational time, yet long enough for the development of thermal pressurization at least in the most catastrophic cases, as shown by previous calculations (Section 4.2, Vardoulakis 2002, Cecinato et al. 2011).

5.1. Choice of parameters

Among all the model parameters listed in Section 4.1, the following are chosen for the parametric study: the slide thickness H and the slope inclination β which are basic geometrical quantities entering classical stability analyses, along with the shearband thickness d, introduced by the thermo-mechanical model. Of the geotechnical properties of

the soil we include κ, λ and Γ, whose range is well established (Section 5.2) and soil permeability k_w. The effects of material friction-softening will be taken into account through the critical state, residual static and residual dynamic friction angles ϕ_{cs}, ϕ_{rs} and ϕ_{rd} as well as the static and dynamic softening rates a_1 and a_2 (c.f. Appendix.) Finally we include the material parameter γ, to explore the impact of the thermo-plastic softening mechanism.

Model parameters that do not exhibit in nature a high variability, or that are not expected to influence the results with their variation, are kept constant in the parametric study. In particular, the soil thermal properties β_s, k_m and C_f are assigned an average value typical of clays (Section 4.2), the Poisson's ratio ν is set equal to an average value of 0.3 and the rate of thermal-friction softening $\tilde{g}$ is set to zero, due to the lack of information on this phenomenon and to its ascertained secondary importance when compared to static and dynamic material friction softening (Cecinato et al. 2011). The reference temperature θ_{ref} is set to 20°C. The compressibility of water c_w, the unit weight of water γ_w and the unit weight of the overburden γ_s are assigned the same values as in Section 4.1, which can be considered representative of average conditions.

5.2. Choice of parameter range

After selecting the variables to be examined in the parametric analysis, realistic ranges for them must be established. We consider $5 \le H \le 250\,\text{m}$, with 5 metres being an arbitrary but reasonable lower-bound value and 250 m representing the maximum depth at which a slip plane has been detected in deep-seated slides (Petley and Allison 1996). The range chosen for the slope inclination is $15° \le \beta \le 35°$ (cf. Cecinato 2009, 2011) while for the shearband thickness $0.3 \le d \le 3\,\text{mm}$ based on the observations by Vardoulakis (2002a) that this value should be a few hundreds of micrometres. Based on the measured properties of typical clay

soils (cf. Schofield and Wroth 1968, Wood et al. 1992), ranges $3\times10^{-2} \le \kappa \le 6\times10^{-2}$, $9\times10^{-2} \le \lambda \le 2.6\times10^{-1}$ and $2.8 \le \Gamma \le 3.8$ can be chosen. The ranges of characteristic friction angles may be determined on the basis of available data from shear tests on clays (cf. Skempton 1985): $20° \le \phi_{cs} \le 32°$, $10° \le \phi_{rs} \le 20°$ and $4° \le \phi_{rd} \le 10°$. Rates of friction-softening, on the other hand, have very rarely been reported in the literature, hence we will select for both a_1 and a_2 a broad range, representing all possible scenarios spanning from the extremely slow to the very sudden softening case: $10^{-5} \le a_1 \le 10^3$, $10^{-5} \le a_2 \le 10^3$. From the few available data on the friction-softening behaviour of clays (Skempton 1985, Lehane and Jardine, 1992 and Tikka and Hutchinson, 1999) it may be deduced that a reasonable mid-range value for both a_1 and a_2 is 0.1, as proposed by Vardoulakis (2002) for the Vajont clay. Permeability is assumed to vary as $10^{-13} \le k_w \le 10^{-6}$ m/s, the upper-bound value representing fissured clays (cf. Powrie 1997) and the lower-bound one representing a uniform clay whose permeability has decreased due to prolonged shearing and consequent alignment of the platy particles parallel to the direction of motion (Vardoulakis 2000). The range chosen for the parameter γ of the thermoplastic model is $10^{-3} \le \gamma \le 10^{-1}$, in agreement with the range of experimentally observed values (Laloui et al. 2008) whilst ensuring the calculation of realistic values for the pressurisation coefficient (cf. Cecinato et al. 2011).

5.3. Parametric analysis setup

The aim of the parametric analysis is to run one simulation for each possible combination of the selected parameters, and analyse the results to determine which factors are most influential in causing large slide velocities. The set of values (levels) that each parameter can assume must be defined. Three levels for each parameter are selected namely the upper-bound, the lower-bound and a mid-range value. This choice is justified by the

likelihood that the parameters investigated will have a more quantifiable effect in the results when they are set to an extreme value, the mid-range setting being useful to evaluate any non-linearity that may arise over each parameter's range. The 13 parameters discussed in Section 5.2 are summarised in Table 3, along with the 3 selected levels denoted as "min", "med", "max".

The parametric study was set up resorting to the concepts of Experimental Design, a branch of Engineering Statistics (e.g. see NIST/SEMATECH 2003) that deals with deliberately changing one or more variables (the selected parameters) in a process (the landslide dynamic simulation), in order to observe the effect that the changes have on a response variable (the calculated velocity 10 seconds after slide initiation). Among the available types of experimental design, the one that was found to best suit the problem at hand due to its robustness, flexibility and simplicity, is the Taguchi method (e.g., Taguchi et al. 1989, Peace 1993). With the current settings of 13 parameters and 3 levels (Table 3), a Taguchi analysis will need only 27 simulations (experiments) to be completed, followed by some basic statistical analysis of the results. By contrast, with the 'full factorial' method (i.e. running a simulation for each one of the possible combinations of parameters) the number of simulations needed would be $3^{13} = 1{,}594{,}323$.

A fundamental step in Taguchi analysis is the definition of a suitable 'orthogonal array', i.e., a 2-dimensional matrix defining the variable settings for each of the experiments needed. Each row of the matrix contains the list of settings for all parameters in one experiment. Each column corresponds to one of the variables, and contains all the values that this variable will be assigned during the experiments. The essential property of the orthogonal array is 'statistical independence': not only within each column an equal number of occurrences for each level is present, but also the columns are mutually orthogonal , i.e. for each level within one column, each level within any other column will occur an equal number of times as well. A given parameter has a strong impact on the

output variable if the results associated with one of its levels are very different from the results associated with another one of its levels. Since, due to orthogonality, the levels of all other parameters occur an equal number of times for each level of this given parameter, their effect will be cancelled out in the computation of the given parameter's effect. The estimation of the effect of any one particular parameter will then tend to be accurate and reproducible (Peace 1993).

The Taguchi method requires to account for any interactions between factors, defined as the situations where two or more factors acting together have a different effect on the output variable than the superposed effects of each factor acting individually. To avoid this complication, the parameters and the relative levels for the analysis at hand were chosen (Section 5.1) with the aim of avoiding interactions. For example, the ranges of the three friction angles ϕ_{cs}, ϕ_{rs} and ϕ_{rd} were chosen contiguous, but not overlapping. Moreover, the lower-bound level of the friction-softening rates a_1 and a_2 was chosen very small but not zero, which would otherwise rule out the effect of the residual friction angles, thus giving rise to an unnecessary interaction.

For the above described 13-parameter, 3-level Taguchi analysis, the conventional orthogonal array "$\mathrm{L}_{27}\left(3^{13}\right)$" is readily available in the literature, and can be filled in with the factors' settings of Table 3 to finalise the parametric study design. The resulting array is shown in Table 4, where a column has been added at the extreme right to specify the output of the simulations for each row, i.e., the calculated slide velocities after 10s from triggering. These rather diverse velocity values constitute the 'raw data' of the Taguchi parametric study, to which some statistical post-processing needs to be applied in order to extract meaningful results. This is done in the next Section.

5.4. Parametric analysis results and discussion

To determine the combination of factors affecting the target variable the most, the velocity output values of Table 4 were interpreted with a level average analysis (Peace 1993), consisting of (1) calculating the average simulation result for each level of each factor, (2) quantifying the effect of each factor by taking the absolute difference between the highest and lowest average results and (3) identifying the strong effects, by ranking the factors from the largest to the smallest absolute difference. Results are summarised in the response table (Table 5).

The top five factors can be reasonably assumed as those having a significant influence in the slide velocity, namely (1) the static friction-softening rate a_1, (2) the slope inclination β, (3) the soil permeability k_w, (4) the dynamic residual friction angle ϕ_{rd} and (5) the slide thickness H. This choice was validated by performing a reliability check (Peace 1993), consisting of calculating an estimate of the predicted response and comparing it with a confirmation run (Table 6) based on the above selected levels of the dominant parameters (Cecinato 2009, 2011).

The worst-case scenario for a planar slide is represented by the parameter combination of Table 6: a potentially unstable slope is bound to be most catastrophic if the soil's static softening rate, the inclination and the thickness of the slope are very large, and the soil's permeability and dynamic residual friction angle are very small. Of these five properties, a_1, β and ϕ_{rd} are not introduced by the consideration of thermal effects, thus constituting important factors in standard landslide analyses as well. The strong influence of a_1 and ϕ_{rd} is explained by observing that while thermal pressurisation needs a certain time to cause significant effective stress reduction, material friction-softening fully develops within centimetres of displacement after the initiation of movement (cf. Section 4.3 and Vardoulakis, 2002). The slope inclination is understandably crucial in the landslide

dynamics as it determines the magnitude of the driving force. On the other hand, parameters k_w and H deserve more attention, as they have been introduced by the thermo-mechanical model and are not normally considered in the analysis of infinite uniform slopes. k_w is the most important one of the two and it affects pore pressure diffusion: a low soil permeability implies poor dissipation of the excess pore pressure within the shearband, thus promoting a sustained reduction of shear resistance. Parameter H on the other hand determines the level of stress, thus affecting the dissipation term D (Section 3.1): the larger H is, the higher the effective stress and therefore the heat production, bringing about a higher pressurization rate that causes a quicker reduction of shear resistance.

The above observations may be useful as guidance for field investigations on potentially unstable large slopes: by measuring or estimating the aforementioned five key properties, it may be possible to estimate whether or not the slope is likely to evolve catastrophically. The slope's inclination and the depth of a potential slip plane may be easier to detect, while for a_1 and ϕ_{rd} it is necessary to collect samples and run laboratory tests, more specifically dynamic ring shear tests such as those performed by Tika and Hutchinson (1999). Although in-situ measurement of the permeability k_w is possible, , the presence of any fractures would lead to an overestimation of its value and in turn to underestimation of thermal pressurisation. Moreover, the permeability of most clays is likely to decrease as the soil approaches residual state, due to the alignment of the platy particles parallel to the direction of motion. Thus, to obtain more sensible information it might be appropriate to run a laboratory permeability test on a sample that has previously undergone prolonged shearing.

6. THE SIGNIFICANCE OF THERMO-MECHANICAL EFFECTS

The analysis of Section 5 involved 13 parameters which can be grouped into 'thermo-mechanical' and 'standard mechanical' parameters, depending on whether or not they are

relevant to a thermo-mechanical analysis only, as opposed to a standard stability analysis. Some of the thermo-mechanical parameters, namely the shearband thickness d and the thermal softening parameter γ, have been left out of the list of key factors, as the level average analysis showed that their influence on model predictions is weak. However, in cases where the standard mechanical parameters assume values that minimise the velocity, such as moderate/absent friction softening and moderate slope angle, the thermo-mechanical factors may yet have an important role in the potential catastrophic evolution of a slide. In order to corroborate the observations of Section 5.4, it is useful to investigate the significance of the thermo-mechanical parameters in particular. This procedure also makes it possible to assess whether these parameters can be decisive in making catastrophic a slide that a standard analysis would predict to be non-catastrophic. The analysis can be performed by means of a standard 4-parameter, 3-level orthogonal array, where the thermo-mechanical factors k_w, H, d, γ are varied within the relevant ranges while the remaining 9 factors of Table 3 are kept constant at mid-level values. To simulate a conservative scenario in terms of loss of resistance to movement, friction-softening is ruled out by setting a_1 and a_2 to zero. With these settings the role of thermo-mechanical phenomena in the catastrophic development of a slide can be explored in isolation.

Given the reduced number of experiments needed, longer simulations could be run, hence the velocity reached by the slide after 10 metres of displacement (cf. Section 5) was here considered as output. The relevant orthogonal array is reported in Table 7.

Next, a level average analysis was carried out, summarised in Table 8, whose outcome confirms the results obtained from the 13-parameter analysis. The resulting order of importance of the thermo-mechanical factors is: (1) permeability, (2) slide thickness, (3) shearband thickness, (4) thermal softening parameter. In fact, the thermo-mechanical parameters alone can make the difference between catastrophic and non-catastrophic evolution of a slide: simulations 7, 8 and 9 in Table 7, in which permeability is high thus

ruling out thermal pressurisation, yield values of velocity after 10m that are below the threshold of 0.05 m/s defining 'very rapid' slides (see Section 5). In contrast, simulations 1-6 of Table 7 can be regarded as cases of 'thermo-mechanical collapse', i.e. cases in which the catastrophic evolution of the slide, when the velocity after 10m exceeds the threshold considered, is brought about by thermo-mechanical phenomena.

It is worth observing that, due to the statistical nature of the results, only about half of the parameters in the ranking can be considered to have a significant effect (Peace 1993). By examining the results of the 4-parameter analysis of this Section in the light of this criterion, we have confirmation that the two properties that should be determined to assess the danger of thermo-mechanical collapse are the permeability of the soil and the thickness of the slide. Both these have a clear physical meaning and are the easiest to quantify among all thermo-mechanical parameters. The measurement of H implies the detection of an existing rupture surface or a reasonable assumption, based on local geology and in-situ conditions, of where a rupture surface would be expected to develop. The permeability k_w can be estimated by specific permeability tests. On the other hand, the shearband thickness has hardly ever been directly measured (e.g. see Morgenstern and Tschalenko 1967, Vardoulakis 2002) and parameter γ would require non-standard thermally-controlled triaxial tests (Laloui and Cekerevac 2003). It may be concluded that, to assess whether a potentially unstable slope is likely to exhibit thermo-mechanical collapse, the depth of the slip plane and the permeability of the soil therein should be estimated or measured.

It may be estimated, as guidance, that if the permeability falls in the (lower) range $10^{-9} \le k_w \le 10^{-13}$ m/s and the depth in the (higher) range $130 \le H \le 250$ m, the likelihood of thermo-mechanical collapse increases; thus the slide could assume unexpectedly high velocities, despite possibly retaining its coherence of mass, and pose a higher threat than a traditional stability analysis would indicate.

It should be finally remarked that while the thermo-mechanical model presented here is useful for estimating the order of magnitude of velocity that a catastrophically collapsing slide can reach after a certain displacement, it cannot be employed to capture the timescale of the creeping motion which sometimes precedes catastrophic collapse in large-scale, deep-seated landslides (e.g. see Veveakis et al. 2007, 2010).

7. CONCLUSIONS

In this work, a new model for the final collapse of planar landslides has been proposed, taking into account a pressurization phase due to frictional heating. It is based on the model presented by Vardoulakis (2002) and a more general and more realistic constitutive law for the soil. The governing equations of the model were integrated numerically and used to analyse the Jiufengershan landslide, demonstrating that realistic predictions for the velocity of the slide can be obtained.

A systematic investigation of the development of catastrophic failure in uniform slopes was then carried out. It was found that the most influential parameters in promoting catastrophic collapse are (1) the static friction-softening rate a_1, (2) the slope inclination β, (3) the soil permeability k_w, (4) the dynamic residual friction angle ϕ_{rd} and (5) the overburden thickness H. The worst case scenario is when a_1, β and H are very large and k_w and ϕ_{rd} are very low. Of the above, the 'thermo-mechanical parameters' k_w and H are not normally considered in standard stability analyses of uniform slopes. A second parametric study demonstrated that thermo-mechanical parameters alone can make the difference between a relatively non-catastrophic event and a catastrophic one. Hence, further insight into the design of landslide risk mitigation measures is gained if, in addition to the standard site investigations, the permeability of the soil is measured and the depth of an existing or expected failure surface is measured or estimated respectively.

ACKNOWLEDGEMENTS

The authors acknowledge the support of the UK's Engineering and Physical Sciences Research Council (EPSRC), grant number EP/C520556/1.

Dr. Emmanuil Veveakis and the late Professor Ioannis Vardoulakis are also gratefully acknowledged for fruitful discussions.

REFERENCES

Alexandre, J., Saboya, F., et al. 1999. Photoacoustic thermal characterization of kaolinite clays. Analyst, **124**(8): 1209-1214.

Baldi, G., Hueckel, T., and Pellegrini, R. 1988. Thermal Volume Changes of the Mineral Water-System in Low-Porosity Clay Soils. Canadian Geotechnical Journal, **25**(4): 807-825.

Campanella, R. G., and Mitchell, J. K. 1968. Influence of temperature variations on soil behavior. Berkeley, University of California, Institute of Transportation and Traffic Engineering, Soil Mechanics and Bituminous Materials Research Laboratory.

Cecinato, F., Zervos, A., Veveakis, E. and Vardoulakis, I. 2008. Numerical modelling of the thermo-mechanical behaviour of soils in catastrophic landslides. *In* Landslides and Engineered Slopes, edited by Z. Chen, et al., pp. 615-621, Taylor and Francis, London.

Cecinato, F. 2009. The Role of Frictional Heating in the Development of Catastrophic Landslides. Ph.D. thesis, 240 pp, School of Civil Engineering and the Environment, University of Southampton (UK).

Cecinato, F. 2011. Mechanics of catastrophic landslides. Lambert Academic Publishing, Saarbrücken.

Cecinato, F., Zervos, A., and Veveakis E. 2011. A thermo-mechanical model for the catastrophic collapse of large landslides. International Journal for Numerical and Analytical Methods in Geomechanics, **35**(14): 1507-1535. doi: 10.1002/nag.963.

Chang, K. J., Taboada, A., and Chan, Y.C. 2005. Analysis of landsliding by earthquake shaking using a block-on-slope thermo-mechanical model: Example of Jiufengershan landslide, central Taiwan. Engineering Geology, **80**(1-2): 151-163.

Ghabezloo, S. and Sulem, J. 2008. Stress dependent thermal pressurization of a fluid-saturated rock. Rock Mechanics and Rock Engineering, **42**:1–24. doi: 10.1007/s00603-008-0165-z.

Habib, P. 1975. Production of gaseous pore pressure during rock slides. Rock Mechanics and Rock Engineering, **7**(4): 193-197.

Hendron, A. J., and Patton, F. D. 1985. The Vaiont slide, a geotehnical analysis based on new geologic observations of the failure surface. Technical Report GL-85-5. Washington, DC, Department of the Army US Corps of Engineers.

Huang, C. C., Lee, Y. H., et al. 2001. Influence of surface-normal ground acceleration on the initiation of the Jih-Feng-Erh-Shan landslide during the 1999 Chi-Chi, Taiwan, earthquake. Bulletin of the Seismological Society of America, **91**(5): 953-958.

Hueckel, T., and Baldi, G. 1990. Thermoplasticity of Saturated Clays - Experimental Constitutive Study. Journal of Geotechnical Engineering-Asce, **116**(12): 1778-1796.

Hueckel, T., and Borsetto, M. 1990. Thermoplasticity of Saturated Soils and Shales - Constitutive-Equations. Journal of Geotechnical Engineering-Asce, **116**(12): 1765-1777.

Hueckel, T. and Pellegrini, R. 1991. Thermoplastic modelling of undrained failure of saturated clay due to heating. Soils and Foundations, **31**(3): 1-16.

IUGS - International working group, L. 1995. A suggested method for describing the rate of movement of a landslide. Bullettin of the International Association of Engineering Geology 52: 75-78.

Lachenbruch, A. H. 1980. Frictional heating, fluid pressure, and the resistance to fault motion. Journal of Geophysical Research, **85**(B11): 6097-6122.

Laloui, L., and Cekerevac, C. 2003. Thermo-plasticity of clays: An isotropic yield mechanism. Computers and Geotechnics, **30**(8): 649-660.

Laloui, L., Cekerevac, C., and Francois, B. 2005. Constitutive modelling of the thermo-plastic behaviour of soils. Revue Europeenne de genie civil, **9**(5-6): 635-650.

Laloui, L., Leroueil, S., and Chalindar, S. 2008. Modelling the combined effect of strain rate and temperature on one-dimensional compression of soils, Canadian Geotechnical Journal, **12**(45): 1765-1777.

Laloui, L., and Francois B. 2009. ACMEG-T: Soil thermoplasticity model. Journal of Engineering Mechanics , **135**(9), 932-944, doi: 10.1061/(ASCE)EM.1943-7889.0000011

Lehane, B. M., and Jardine, R. J. 1992. Residual Strength Characteristics of Bothkennar Clay. Geotechnique, **42**(2): 363-367.

Marques, M. E. S., Leroueil, S., and Almeida, M. S. S. 2004. Viscous behaviour of St-Roch-de-l'Achigan clay, Quebec. Canadian Geotechnical Journal, **41**(1): 25-38.

Modaressi, H. and Laloui, L. 1997. A thermo-viscoplastic constitutive model for clays. International Journal for Numerical and Analytical Methods in Geomechanics, **21**(5): 313-335.

Morgenstern, N. R., and Tschalenko, J. S. 1967. Microscopic structures in kaolin subjected to direct shear. Géotechnique, **17**(4): 309-328.

Newmark, N. 1965. Effects of earthquakes on dams and embankments. Geotechnique, **15**(2): 139-160**.**

NIST/SEMATECH. 2003. e-Handbook of Statistical Methods. Available from http://www.itl.nist.gov/div898/handbook/ [accessed 23/06/2010].

Peace, G. S. 1993. Taguchi methods : a hands-on approach. Addison-Wesley, Reading, Massachussets.

Petley, D. N. and Allison, R. J. 1997. The mechanics of deep-seated landslides. Earth Surface Processes and Landforms **22**(8): 747-758.

Powrie, W. 1997. Soil mechanics : concepts and applications. E & FN Spon, London; New York.

Rice, J. R. 2006. Heating and weakening of faults during earthquake slip. Journal of Geophysical Research-Part B-Solid Earth, **111**, B05311, doi:10.1029/2005JB004006.

Roscoe, K. H., and Burland, J. B. 1968. On the generalized stress-strain behavior of 'wet' clay, in J. Heyman and F. A. Leckie (eds.), Engineering plasticity (Cambridge University Press), pp. 535-609.

Schofield, A. N., and Wroth, C. P. 1968. Critical State Soil Mechanics. McGraw Hill, London.

Shou, K. J., and Wang, C. F. 2003. Analysis of the Chiufengershan landslide triggered by the 1999 Chi-Chi earthquake in Taiwan. Engineering Geology, **68**(3-4): 237-250.

Sibson, R. H., 1973. Interaction between temperature and pore-fluid pressure during earthquake faulting: a mechanism for partial or total stress relief. Nature, **243**, 66-68.

Skempton, A. W. 1985. Residual Strength of Clays in Landslides, Folded Strata and the Laboratory. Geotechnique, **35**(1): 3-18.

Sulem, J., Lazar, P., and Vardoulakis, I. 2007. Thermo-poro-mechanical properties of clayey gouge and application to rapid fault shearing. International Journal for Numerical and Analytical Methods in Geomechanics, **31**(3): 523-540.

Sultan, N. 1997. Etude du comportement thermo-mèchanique de l'argile de Boom: expériences et modélisation. PhD thesis, ENPC, Paris, CERMES.

Sultan, N., Delage, P., and Cui, Y. J. 2002. Temperature effects on the volume change behaviour of Boom clay. Engineering Geology, **64**(2-3): 135-145.

Taguchi, G., El Sayed, M., and Hsaing, C. 1989. Quality Engineering and quality systems. McGraw-Hill, New York.

Tika, T. E. and Hutchinson, J. N. 1999. Ring shear tests on soil from the Vaiont landslide slip surface. Geotechnique, **49**(1): 59-74.

Vardoulakis, I. 2000. Catastrophic landslides due to frictional heating of the failure plane. Mechanics of Cohesive-Frictional Materials, **5**(6): 443-467.

Vardoulakis, I. 2001. Thermo-poro-mechanical analysis of rapid fault deformation. *In* Proceedings of the International Conference on Micromechanics of Granular Media, Sendai, Japan. Balkema, Rotterdam.

Vardoulakis, I. 2002. Dynamic thermo-poro-mechanical analysis of catastrophic landslides. Geotechnique **52**(3): 157-171.

Veveakis, E., Vardoulakis, I., and Di Toro, G. 2007. Thermoporomechanics of creeping landslides: The 1963 Vaiont slide, northern Italy. Journal of Geophysical Research-Earth Surface, **112**(F3).

Veveakis, E., Alevizos, S., and Vardoulakis, I. 2010. Chemical reaction capping of thermal instabilities during shear of frictional faults. Journal of the Mechanics and Physics of Solids, **58**: 1175-1194.

Voight, B., and Faust, C. 1982. Frictional Heat and Strength Loss in Some Rapid Landslides. Geotechnique, **32**(1): 43-54.

Wang, W. N., Chigira, M., and Furuya, T. 2003. Geological and geomorphological precursors of the Chiu-fen-erh-shan landslide triggered by the Chi-chi earthquake in central Taiwan. Engineering Geology, **69**(1-2): 1-13.

Wibberley, C. A. J. and Shimamoto, T. 2005. Earthquake slip weakening and asperities explained by thermal pressurization. Nature **436**(7051): 689-692.

Wood, D. M., Mackenzie, N. L. and Chan, A. H. C. 1992. Selection of parameters for numerical predictions. *In* Predictive soil mechanics, Proceedings of the Wroth memorial Symposium St Catherine College, Oxford, pp 496-512, Thomas Telford, London.

TABLES

Table 1. Field data of Jiufengershan slide.

Unit weight of water	γ_w	$9.81*10^3$	N/m^3
Unit weight of the overburden	γ_s	$24.525*10^3$	N/m^3
Slope inclination	β	20	degrees
Slide thickness	H	50	m
Average shearband thickness	d	$1*10^{-2}$	m
Height of water table	h_w	30	m

Table 2. Choice of parameters for Jiufengershan slide.

Slope of URL of clay	κ	$4.5*10^{-2}$	-----
Slope of NCL of clay	λ	0.17	-----
Specific volume intercept of clay	Γ	3.2	kPa
Soil (drained) Poisson's ratio	v	0.3	-----
Compressibility of water	c_w	$4.93*10^{-4}$	MPa^{-1}
Reference temperature	θ_{ref}	25	°C
Soil thermal diffusivity coefficient	k_m	$1.45*10^{-7}$	m^2/s
Thermo-elastic expansion coefficient	β_s	$7.41*10^{-5}$	$°C^{-1}$
Thermal constant	C_f	2.84	Mpa/°C
Soil permeability	k_w	10^{-11}	m/s
Thermal softening parameter	γ	10^{-2}	-----
Calculated friction angle at CS	ϕ'_{cs}	27.4	degrees
Calculated initial normal effective stress	σ_n'	0.876	MPa

Table 3. Parameters selected for the parametric study and their levels.

Parameter	Level			Units
	min	med	max	
Slope inclination: β	15	25	35	degrees
permeability: k_w	10^{-13}	10^{-9}	10^{-6}	m/s
Slide thickness: H	5	130	250	m
Slip zone thickness: d	0.3	1	3	mm
Th. softening parameter: γ	10^{-3}	10^{-2}	10^{-1}	-----
Critical state fric. angle.: φ_{cs}	20	25	32	degrees
Static res. fric. angle: φ_{rs}	10	15	20	degrees
Dynamic res. fric. angle: φ_{rd}	4	8	10	degrees
Static softening parameter: a_1	10^{-5}	10^{-1}	10^{3}	-----
Dynamic softening parameter: a_2	10^{-5}	10^{-1}	10^{3}	-----
Specific volume intercept: Γ	2.8	3.2	3.8	-----
Slope of κ-line: κ	3×10^{-2}	4.5×10^{-2}	6×10^{-2}	-----
Slope of λ-line: λ	9×10^{-2}	1.7×10^{-1}	2.6×10^{-1}	-----

Table 4. Orthogonal array for the 13-parameter Taguchi analysis.

Exp/param	β	k_w	H	d	γ	φ_{cs}	φ_{rs}	φ_{rd}	a_1	a_2	Γ	k	λ	Results: velocity after 10s (m/s)
1	15	1.00E-13	5	3.00E-04	1.00E-03	20	10	4	1.00E-05	1.00E-05	2.8	3.00E-02	9.00E-02	1.52
2	15	1.00E-13	5	3.00E-04	1.00E-02	25	15	8	1.00E-01	1.00E-01	3.2	4.50E-02	1.70E-01	17.94
3	15	1.00E-13	5	3.00E-04	1.00E-01	32	20	10	1.00E+03	1.00E+03	3.8	6.00E-02	2.60E-01	18.68
4	15	1.00E-09	130	1.00E-03	1.00E-03	20	10	8	1.00E-01	1.00E-01	3.8	6.00E-02	2.60E-01	17.24
5	15	1.00E-09	130	1.00E-03	1.00E-02	25	15	10	1.00E+03	1.00E+03	2.8	3.00E-02	9.00E-02	18.55
6	15	1.00E-09	130	1.00E-03	1.00E-01	32	20	4	1.00E-05	1.00E-05	3.2	4.50E-02	1.70E-01	2.32
7	15	1.00E-06	250	3.00E-03	1.00E-03	20	10	10	1.00E+03	1.00E+03	3.2	4.50E-02	1.70E-01	13.45
8	15	1.00E-06	250	3.00E-03	1.00E-02	25	15	4	1.00E-05	1.00E-05	3.8	6.00E-02	2.60E-01	0.85
9	15	1.00E-06	250	3.00E-03	1.00E-01	32	20	8	1.00E-01	1.00E-01	2.8	3.00E-02	9.00E-02	18.69
10	25	1.00E-13	130	3.00E-03	1.00E-03	25	20	4	1.00E-01	1.00E+03	2.8	4.50E-02	2.60E-01	29.25
11	25	1.00E-13	130	3.00E-03	1.00E-02	32	10	8	1.00E+03	1.00E-05	3.2	6.00E-02	9.00E-02	33.45
12	25	1.00E-13	130	3.00E-03	1.00E-01	20	15	10	1.00E-05	1.00E-01	3.8	3.00E-02	1.70E-01	13.75
13	25	1.00E-09	250	3.00E-04	1.00E-03	25	20	8	1.00E+03	1.00E-05	3.8	3.00E-02	1.70E-01	20.02
14	25	1.00E-09	250	3.00E-04	1.00E-02	32	10	10	1.00E-05	1.00E-01	2.8	4.50E-02	2.60E-01	7.8
15	25	1.00E-09	250	3.00E-04	1.00E-01	20	15	4	1.00E-01	1.00E+03	3.2	6.00E-02	9.00E-02	33.36
16	25	1.00E-06	5	1.00E-03	1.00E-03	25	20	10	1.00E-05	1.00E-01	3.2	6.00E-02	9.00E-02	4.00E-05
17	25	1.00E-06	5	1.00E-03	1.00E-02	32	10	4	1.00E-01	1.00E+03	3.8	3.00E-02	1.70E-01	35.85
18	25	1.00E-06	5	1.00E-03	1.00E-01	20	15	8	1.00E+03	1.00E-05	2.8	4.50E-02	2.60E-01	12.15
19	35	1.00E-13	250	1.00E-03	1.00E-03	32	15	4	1.00E+03	1.00E-01	2.8	6.00E-02	1.70E-01	53.25
20	35	1.00E-13	250	1.00E-03	1.00E-02	20	20	8	1.00E-05	1.00E+03	3.2	3.00E-02	2.60E-01	33.89
21	35	1.00E-13	250	1.00E-03	1.00E-01	25	10	10	1.00E-01	1.00E-05	3.8	4.50E-02	9.00E-02	45.4
22	35	1.00E-09	5	3.00E-03	1.00E-03	32	15	8	1.00E-05	1.00E+03	3.8	4.50E-02	9.00E-02	1.11
23	35	1.00E-09	5	3.00E-03	1.00E-02	20	20	10	1.00E-01	1.00E-05	2.8	6.00E-02	1.70E-01	0.69
24	35	1.00E-09	5	3.00E-03	1.00E-01	25	10	4	1.00E+03	1.00E-01	3.2	3.00E-02	2.60E-01	48.38
25	35	1.00E-06	130	3.00E-04	1.00E-03	32	15	10	1.00E-01	1.00E-05	3.2	3.00E-02	2.60E-01	34.53
26	35	1.00E-06	130	3.00E-04	1.00E-02	20	20	4	1.00E+03	1.00E-01	3.8	4.50E-02	9.00E-02	45.51
27	35	1.00E-06	130	3.00E-04	1.00E-01	25	10	8	1.00E-05	1.00E+03	2.8	6.00E-02	1.70E-01	2.58

Table 5. Response of the level average analysis for the 13-parameter Taguchi analysis.

RESPONSE TABLE (slide velocity in m/s after t=10 seconds from triggering)													
Level/par.	**β**	**k_w**	**H**	**d**	**γ**	**φ_{cs}**	**φ_{rs}**	**φ_{rd}**	**a_1**	**a_2**	**Γ**	**k**	**λ**
Min	12.14	27.46	15.15	20.22	18.93	19.06	21.53	27.81	7.09	16.77	16.05	25.02	21.95
Med	20.63	16.61	21.91	24.29	21.61	20.33	20.61	17.45	25.88	24.73	22.83	19.44	17.76
Max	29.48	18.18	25.19	17.74	21.70	22.85	18.78	16.98	29.27	20.75	22.05	17.79	22.53
Effect of parameter (Delta)	**17.34**	**10.85**	**10.04**	**6.56**	**2.77**	**3.79**	**2.74**	**10.83**	**22.18**	**7.96**	**6.77**	**7.23**	**4.77**
Ranking	**2**	**3**	**5**	9	12	11	13	**4**	**1**	6	8	7	10

Table 6. Parameter settings for the confirmation run of the 13-parameter Taguchi analysis.

Exp/param	β_{max}	$k_{w,min}$	H_{max}	d_{med}	γ_{med}	$\varphi_{cs,med}$	$\varphi_{rs,med}$	$\varphi_{rd,min}$	$a_{1,max}$	$a_{2,med}$	Γ_{med}	k_{med}	λ_{med}	Result: velocity v after 10s (m/s)
Confirmation run	35	1.00E-13	250	1.00E-003	1.00E-002	25	15	4	1.00E+03	0.1	3.2	4.50E-02	1.70E-01	51.2

Table 7. Orthogonal array for the 4-parameter Taguchi analysis.

Exp/param	k_w	H	d	Γ	velocity at 10m (m/s)
1	1.00E-013	5	3.00E-004	1.00E-003	1.46
2	1.00E-013	130	1.00E-003	1.00E-002	6.02
3	1.00E-013	250	3.00E-003	1.00E-001	5.2
4	1.00E-009	5	1.00E-003	1.00E-001	0.82
5	1.00E-009	130	3.00E-003	1.00E-003	3.8
6	1.00E-009	250	3.00E-004	1.00E-002	1.97
7	1.00E-006	5	3.00E-003	1.00E-002	0.03
8	1.00E-006	130	3.00E-004	1.00E-001	1.62E-03
9	1.00E-006	250	1.00E-003	1.00E-003	1.23E-03

Table 8. Response of the level average analysis for the 4-parameter Taguchi analysis.

RESPONSE TABLE (slide velocity after 10m displacement)				
Lev/param	**k_w**	**H**	**d**	**γ**
Min	4.227	0.770	1.144	1.754
Med	2.197	3.274	2.280	2.673
Max	0.011	2.390	3.010	2.007
Effect of parameter (Delta)	**4.216**	**2.504**	**1.866**	**0.920**
ranking	**1**	**2**	**3**	**4**

FIGURE CAPTIONS

Figure 1. Infinite slope geometry. The shearband (shaded) has negligible thickness compared to that of the overburden, i.e. $H>>d$. The slope inclination with respect to horizontal is β.

Figure 2. Temperature isochrones for the catastrophic collapse phase of the Jiufengershan slide, with shearband thickness d=1cm.

Figure 3. Excess pore pressure isochrones for the catastrophic collapse phase of the Jiufengershan slide, with shearband thickness d=1cm.

Figure 4. Computed shear stress and excess pore pressure at the shearband mid-plane of the Jiufengershan slide as a function of time, with shearband thickness d=1cm.

Figure 5. Computed velocity and displacement profiles of the Jiufengershan slide, with shearband thickness d=1cm.

Figure 6. Computed velocity and displacement of the Jiufengershan slide, plotted against time, with shearband thickness d=1cm. The vertical dashed line marks the reaching of 1km of displacement, roughly corresponding to a velocity of 80 m/s.

Figure 7. Computed shear stress and excess pore pressure at the shearband mid-plane of the Jiufengershan slide as a function of time, in the case of friction-softening soil, with shearband thickness d=1cm.

Figure 8. Computed temperature at the shearband mid-plane of the Jiufengershan slide as a function of time, in the case of friction-softening soil, with shearband thickness *d*=1cm.

Figure 9. Computed velocity and displacement of the Jiufengershan slide, plotted against time for the first 20 seconds of catastrophic collapse, in the case of friction-softening soil, with shearband thickness *d*=1cm.

Figure 10. Temperature isochrones for the Jiufengershan slide in the case of thinner shearband (*d*=1mm instead of 1cm).

Figure 11. Excess pore pressure isochrones for the Jiufengershan slide in the case of thinner shearband (*d*=1mm instead of 1cm).

Figure 12. Computed shear stress and excess pore pressure at the shearband mid-plane of the Jiufengershan slide as a function of time, in the case of thinner shearband (*d*=1mm instead of 1cm).

Figure 13. Computed velocity of the Jiufengershan slide in the case of thinner shearband (*d*=1mm instead of 1cm).

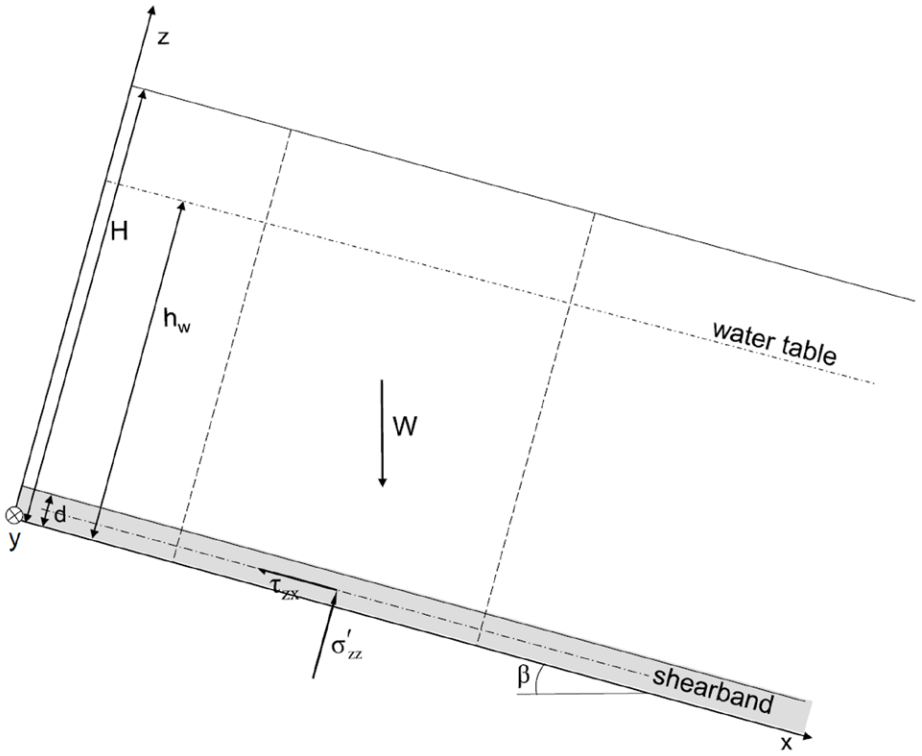
z
H
h_w
water table
W
d
y
τ_{zx}
σ'_{zz}
β
shearband
x

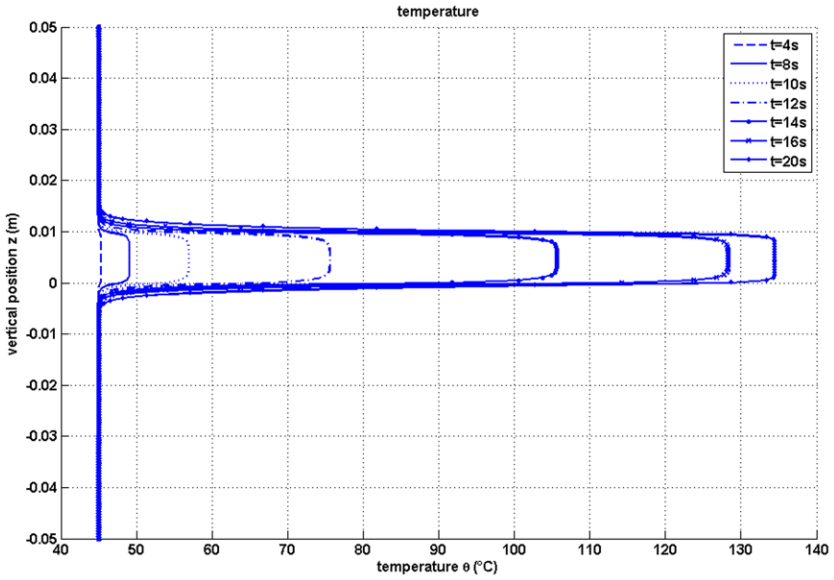
temperature
t=4s
t=8s
t=10s
t=12s
t=14s
t=16s
t=20s
vertical position z (m)
0.05
0.04
0.03
0.02
0.01
0
-0.01
-0.02
-0.03
-0.04
-0.05
40
50
60
70
80
90
100
110
120
130
140
temperature θ (°C)

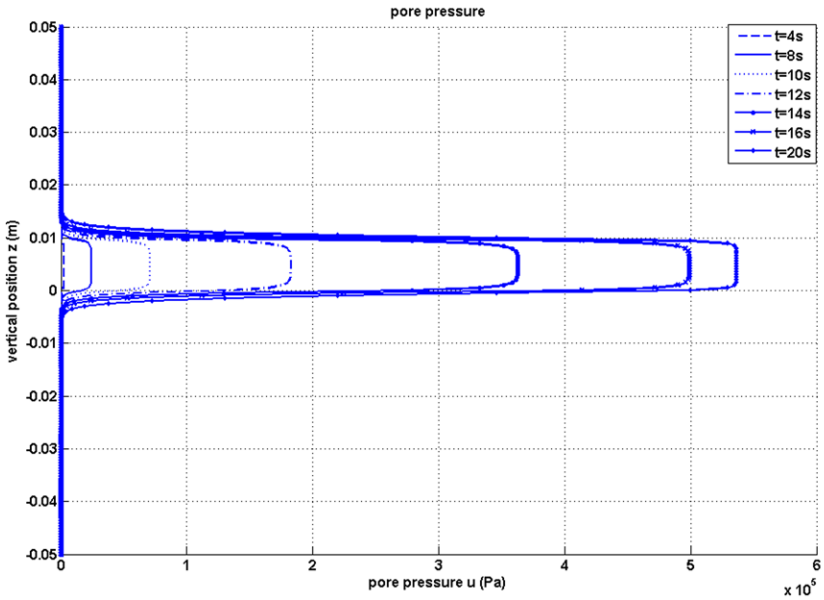
pore pressure
t=4s
t=8s
t=10s
t=12s
t=14s
t=16s
t=20s
vertical position z (m)
0.05
0.04
0.03
0.02
0.01
0
-0.01
-0.02
-0.03
-0.04
-0.05
0
1
2
3
4
5
6
pore pressure u (Pa)
x 10^5

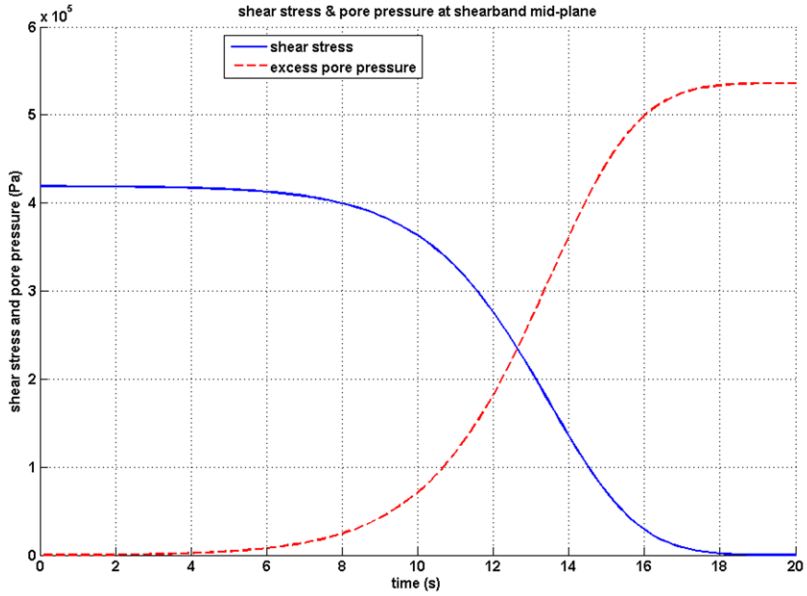
shear stress & pore pressure at shearband mid-plane
x 10^5
shear stress
excess pore pressure
shear stress and pore pressure (Pa)
6
5
4
3
2
1
0
0
2
4
6
8
10
12
14
16
18
20
time (s)

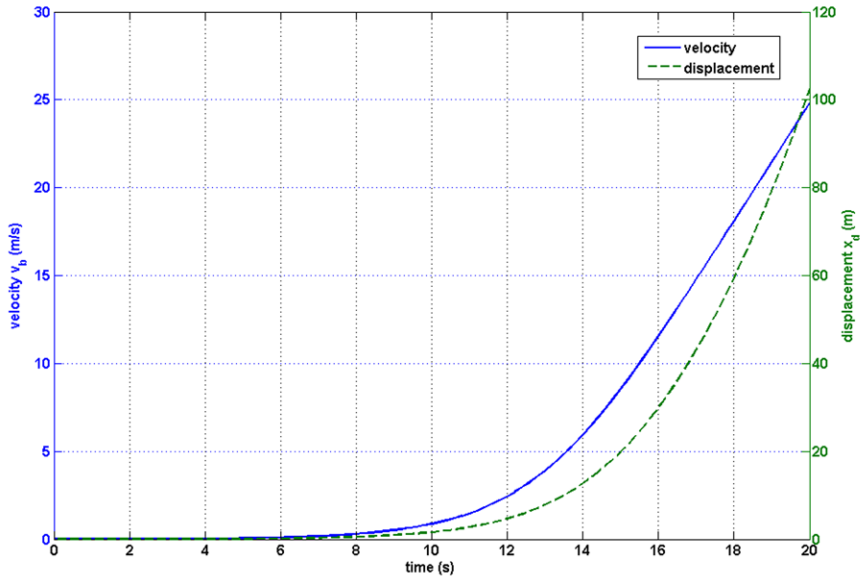
velocity
displacement
velocity v_b (m/s)
displacement x_d (m)
time (s)

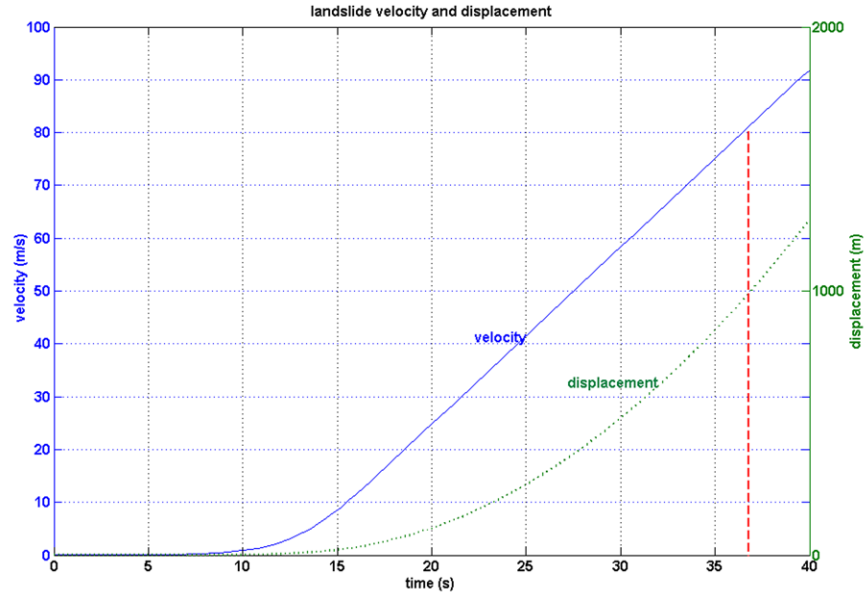
landslide velocity and displacement
velocity (m/s)
displacement (m)
velocity
displacement
time (s)

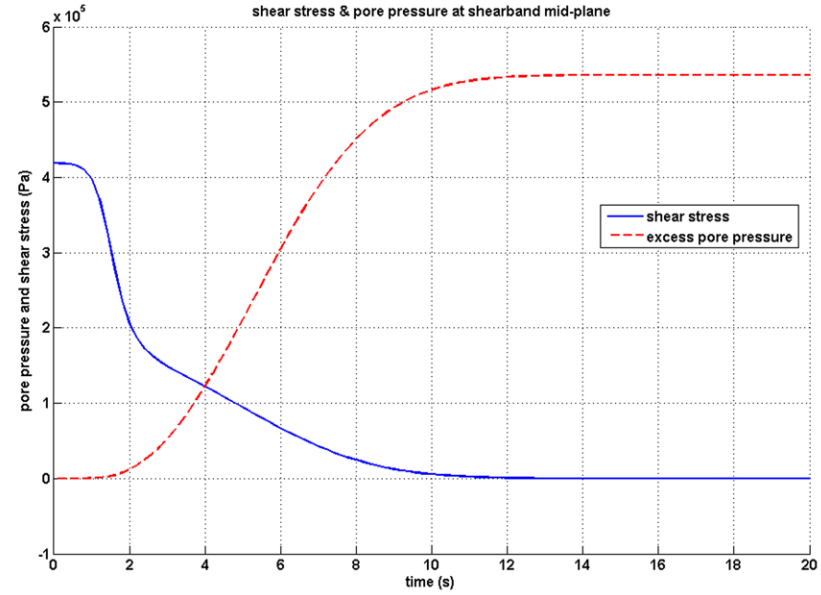
shear stress & pore pressure at shearband mid-plane
x 10^5
pore pressure and shear stress (Pa)
time (s)
shear stress
excess pore pressure

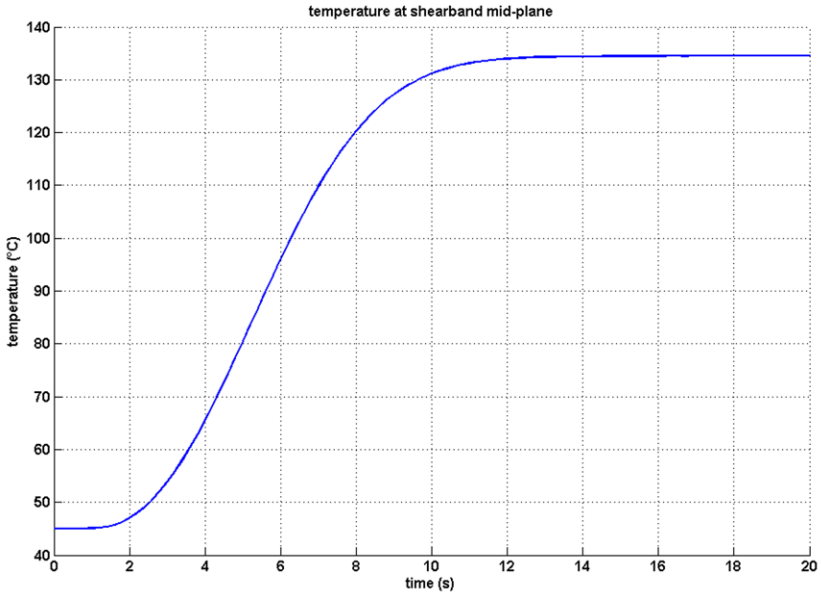
temperature at shearband mid-plane
temperature (°C)
time (s)

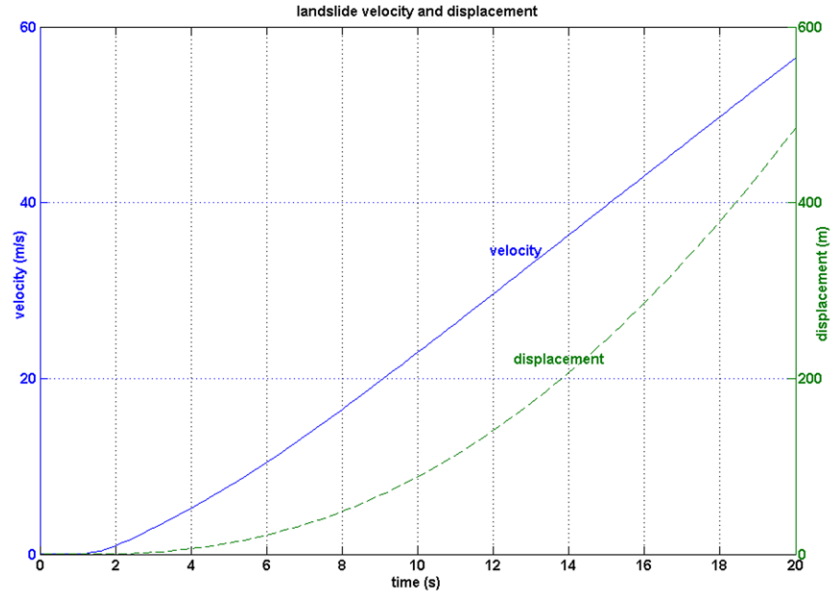
landslide velocity and displacement
velocity (m/s)
displacement (m)
time (s)
velocity
displacement
0
20
40
60
0
200
400
600
0
2
4
6
8
10
12
14
16
18
20

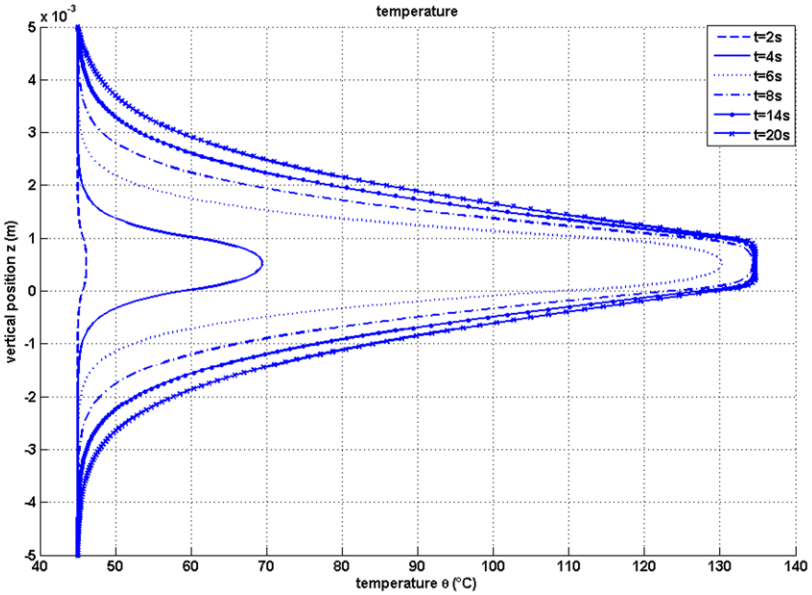
temperature
x 10^-3
vertical position z (m)
temperature θ (°C)
t=2s
t=4s
t=6s
t=8s
t=14s
t=20s
5
4
3
2
1
0
-1
-2
-3
-4
-5
40
50
60
70
80
90
100
110
120
130
140

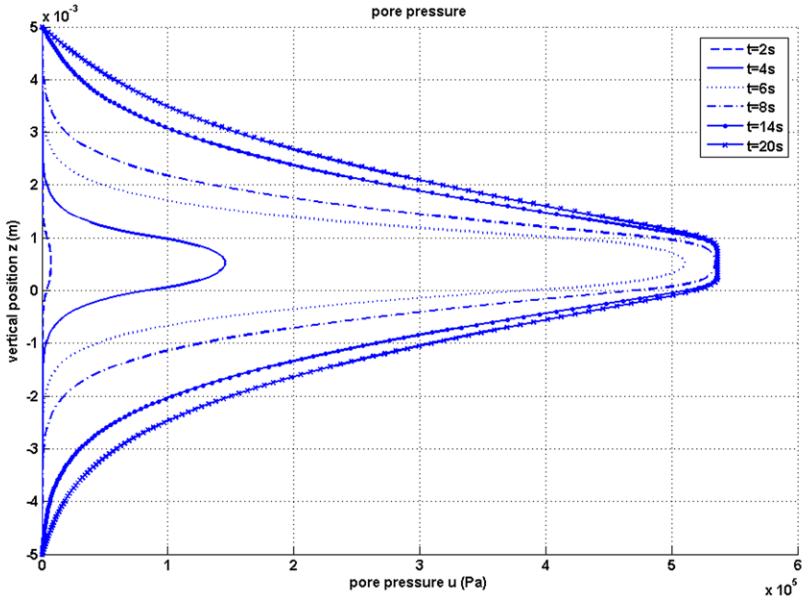
pore pressure
x 10^-3
vertical position z (m)
pore pressure u (Pa)
x 10^5
t=2s
t=4s
t=6s
t=8s
t=14s
t=20s

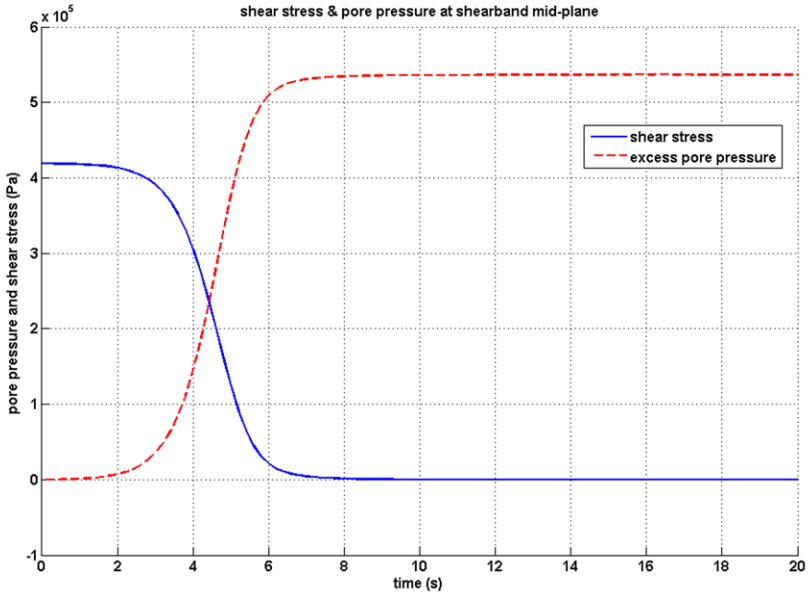
shear stress & pore pressure at shearband mid-plane
x 10^5
pore pressure and shear stress (Pa)
time (s)
shear stress
excess pore pressure

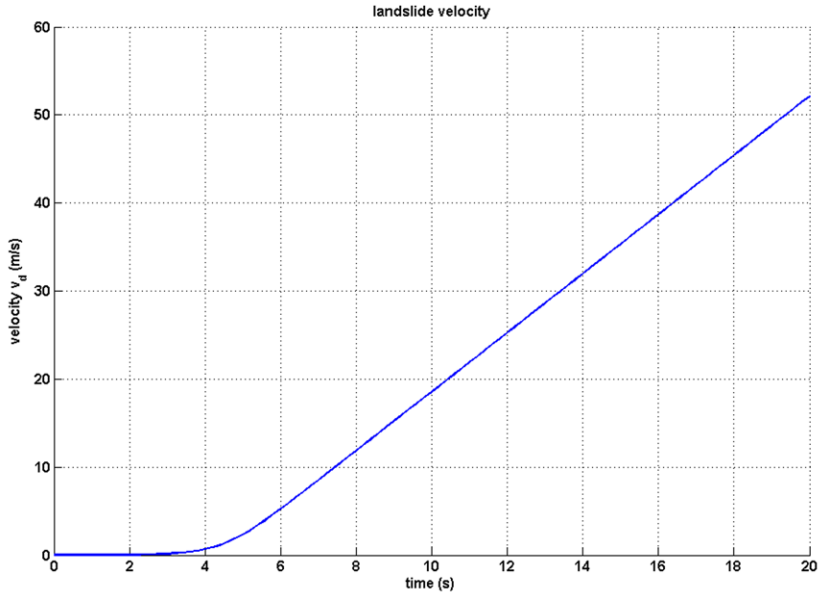
landslide velocity
velocity v_d (m/s)
time (s)
0
10
20
30
40
50
60
0
2
4
6
8
10
12
14
16
18
20

APPENDIX

In critical state soil mechanics the parameter M is constant and depends on the soil's friction angle at critical state. However, to account for the reduction of the friction angle of clays when they reach the so-called residual state, the hyperbolic strain- and strain-rate softening law proposed by Vardoulakis (2002) is adopted. Furthermore, we allow for possible thermal-friction softening behavior as in Section 2.1. Therefore in the general case the critical state parameter M, which can be related to the friction angle at critical state φ'_{cs}, is taken to depend on strain, strain-rate and temperature as (Cecinato et al., 2011):

[1] $$M(\gamma,\dot{\gamma},\theta) = \hat{M}\left(\gamma,\dot{\gamma}\right) - \tilde{g}\left(\theta-\theta_{ref}\right)$$

where the material-friction softening critical state parameter $\hat{M}$ is expressed as (Cecinato, 2009):

[2] $$\hat{M} = \sqrt{3}\sin\left[\arctan\left(\hat{\mu}\right)\right]$$

In the above, the friction coefficient $\hat{\mu}\left(\gamma,\dot{\gamma}\right)$ follows the static and dynamic friction-softening law of Vardoulakis (2002):

[3] $$\hat{\mu} = \mu_r + \left(\mu_p - \mu_r\right)\frac{1}{1+a_1\dfrac{x_d}{d}}$$

where

[4] $$\mu_r = \mu_{rd} + (\mu_{rs} - \mu_{rd}) \frac{1}{1 + a_2 \frac{v_d}{d}}$$

In the above d is the shearband thickness, x_d the slide displacement and v_d the slide velocity, so that the (thickness-dependent) shear strain is $\gamma = \frac{x_d}{d}$ and its rate $\dot{\gamma} = \frac{v_d}{d}$. The limiting values μ_{rs} and μ_{rd} are respectively the static and dynamical residual friction coefficients, while μ_p is the initial value of friction coefficient and a_1, a_2 are numerical factors defining how quickly the static and dynamic coefficients respectively decrease with displacement and velocity.

The critical state parameter $M(\gamma, \dot{\gamma}, \theta)$ features in the heat equation [5] via parameter F_i (Cecinato et al., 2011).